Volume 27
Number 44
28 November 2025
Pages 7103–7238

CrystEngComm

rsc.li/crystengcomm

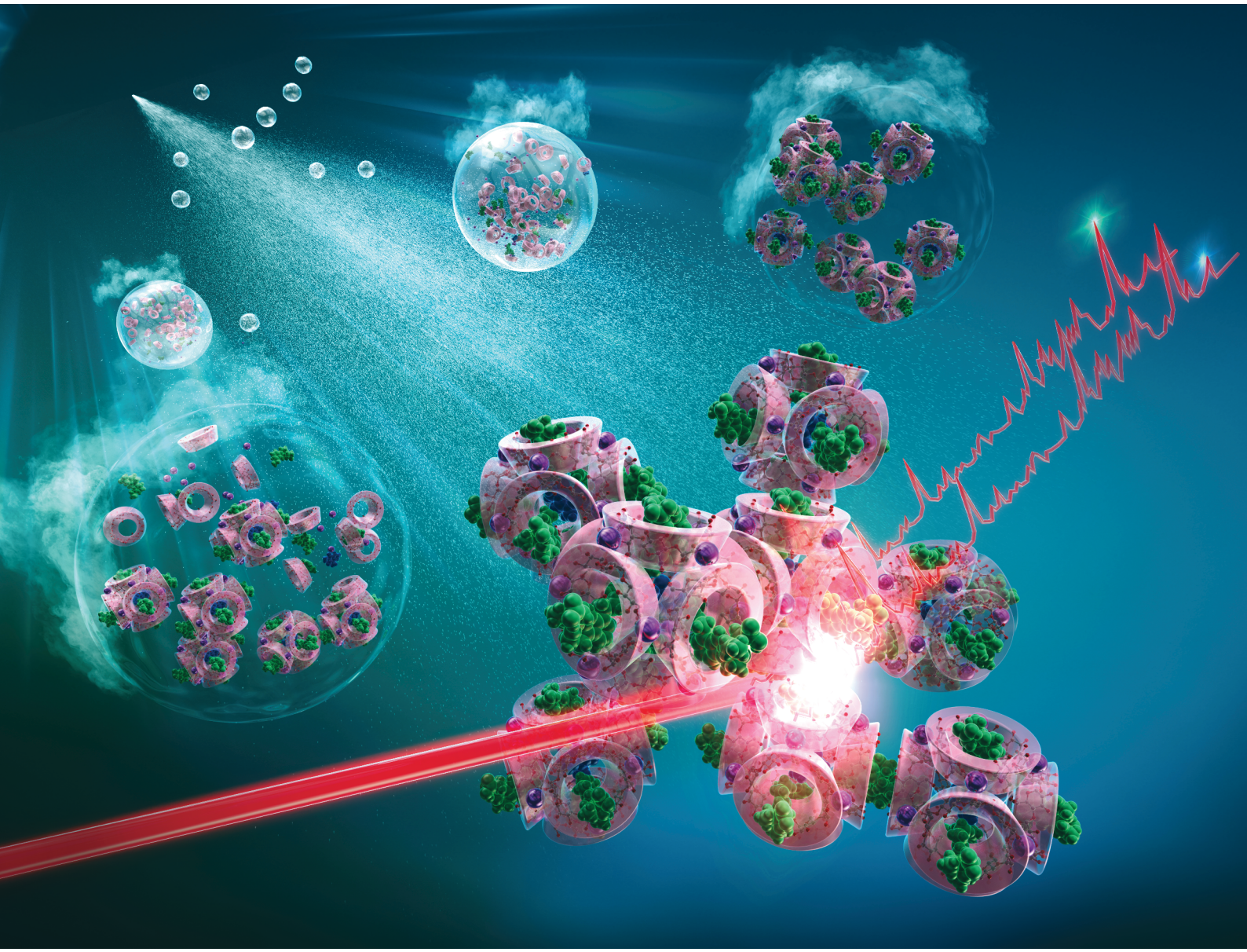

ISSN 1466-8033

ROYAL SOCIETY OF CHEMISTRY

PAPER

Kazunori Kadota *et al.*

Physically stable cyclodextrin metal–organic frameworks formed *via* a drug-assisted amorphous to crystal phase transition

CrystEngComm

ROYAL SOCIETY OF CHEMISTRY

PAPER

View Article Online
View Journal | View Issue

Cite this: *CrystEngComm*, 2025, **27**, 7121

Physically stable cyclodextrin metal–organic frameworks formed *via* a drug-assisted amorphous to crystal phase transition

Ryoma Tanaka, [a] Miki Nagatani,[a] Ryuta Togashi,[c] Katsuhiko Minoura,[a] Hiromasa Uchiyama, [a] Shunsuke Tanaka, [c] Yuichi Tozuka*[a] and Kazunori Kadota *[ab]

Received 28th July 2025,
Accepted 6th October 2025

DOI: 10.1039/d5ce00755k

rsc.li/crystengcomm

Formation of cyclodextrin metal–organic frameworks (CD-MOFs) for drug-loading applications is challenging due to the long preparation time and low loading capacity. In this study, the amorphous–crystal phase transition in CD-MOFs during spray drying was exploited to efficiently synthesize drug-loaded CD-MOFs by incorporating hydrophobic etodolac (ETD) and hydrophilic theophylline (THP) molecules. Spray drying of a precursor mixture consisting of ETD and/or THP, along with CD-MOF components (γ-CD and KOH) in 40% ethanol, was completed within 30 min. Rapid solvent evaporation during the spray drying process enabled the incorporation of ETD and THP molecules into the slightly crystalline CD-MOF particles, resulting in high drug loading (>90% w/w). The mechanistic understanding of CD-MOF formation in the presence of drugs was elucidated based on the solution-phase interactions and solid-state configurations using NMR and Raman spectroscopies, respectively. More importantly, ETD molecules within CD-MOF cavities act as linkers between γ-CD units, thereby contributing to the structural formation and enhancing the physical stability of the CD-MOFs. Our study demonstrates the potential of spray-drying for large-scale production of CD-MOFs for pharmaceutical applications.

Introduction

Metal–organic frameworks (MOFs), which are coordination compounds between organic linkers and metal ions, have emerged as a new class of crystalline porous materials.[1] MOFs have many applications, including gas adsorption/separation,[2,3] catalysis,[4] and drug delivery.[5] Specifically, γ-cyclodextrin (γ-CD) and potassium (K^+) ions are used to build "green" CD-based MOFs (CD-MOFs), and the crystalline structure is interesting in the pharmaceutical field due to their good biocompatibility and medical applications as a nano-carrier.[6,7] CD-MOFs exhibit a body-centered cubic packing arrangement constructed from $(\gamma\text{-CD})_6$ cubes linked with the coordinate bond between the hydroxyl group of γ-CD and K^+ ions.[8,9] The cubic crystal has a central cavity and linker sections which provide hydrophobic and hydrophilic spaces, respectively (Scheme 1A).

There have been significant achievements in the design of CD-MOFs.[10–12] For instance, CD-MOFs can be synthesized by vapor diffusion method.[11,13] The preferential volatilization of suitable solvent enriches the chamber, and the vapor slowly

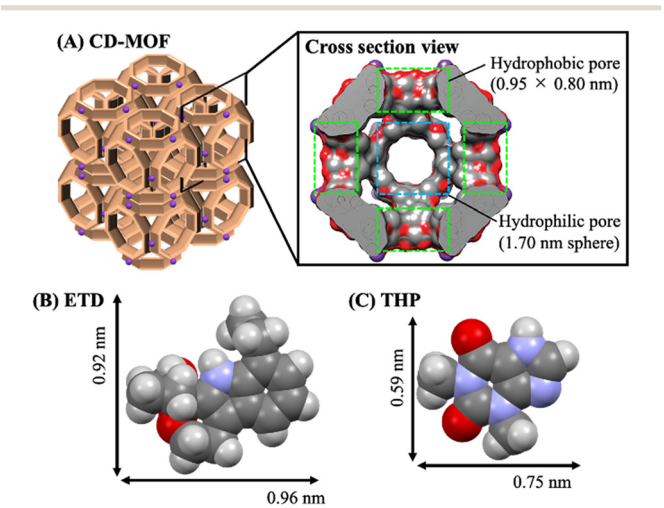

Scheme 1 Representation of the crystalline structure of (A) CD-MOF and cubic $(\gamma\text{-CD})_6$ unit which was cut away to reveal the inner pore (refcode: LAJLAL), (B) ETD (refcode: JUKNAH), and (C) THP (refcode: BAPLOT01) in a space-filling model.

[a] *Faculty of Pharmacy, Osaka Medical and Pharmaceutical University, 4-20-1 Nasahara, Takatsuki, Osaka 569-1094, Japan. E-mail: yuichi.tozuka@ompu.ac.jp; Fax: +81 72 690 1218*
[b] *School of Pharmaceutical Sciences, Wakayama Medical University, 25-1 Shichiban-cho, Wakayama, Wakayama 640-8156, Japan. E-mail: kazunori-kadota@wakayama-med.ac.jp; Tel: +81 734 98 7644*
[c] *Faculty of Environmental and Urban Engineering, Kansai University, 3-3-35 Yamate-cho, Suita, Osaka 564-8680, Japan*

diffuses into a polar solution, such as γ-CD and KOH, leading to the slow crystallization of CD-MOFs. Anti-solvent crystallization is another method in which CD-MOFs are crystallized by adding an anti-solvent followed by stirring for shorter preparation time.[11,14] Both methods take several days to weeks and the produced CD-MOF carrier results in low drug content yield.[13,14] In a recent paper, CD-MOF has been utilized for multi-drug transport with experimental and simulation studies; however, the prepared CD-MOF by slow vapor diffusion required 10 days of preparation and exhibited low drug loading.[15] While these methods are suitable for small-scale preparation, they are not amenable to commercial manufacturing.

Scalable spray drying, a widely used and adaptable technique in pharmaceutical manufacturing, has frequently been demonstrated to enable the formation of CD-based inclusion powders.[16,17] Nevertheless, there are only a few reports on the preparation of CD-MOFs by spray drying. We previously documented that the crystallization of CD-MOFs can be effectively promoted by leveraging the poor solvent effect during spray drying, thereby enabling controlled drug release from CD-MOFs.[18,19] In case of conventional MOFs (without CD), amorphous MOFs are crystallized by the self-assembly of metal ions and organic ligands facilitated by the addition of ethanol.[20,21] Similar phase transition in MOF from amorphous to crystalline was triggered by mechanochemical stress, solvent absorption, and heat.[22–24] The partially crystalline MOFs have been applied to gas absorption/separation because of their flexible structure and excellent size selectivity.[25,26]

We hypothesize that the amorphous–crystal transition in CD-MOFs during spray drying in the presence of drug molecules leads to the formation of slightly crystalline CD-MOFs, in which the framework assembles while simultaneously incorporating the drug molecules. This process would generate low-density pores within the central and linker regions of the $(\gamma\text{-CD})_6$ cubic crystal, enabling the effective containment of drug molecules. Therefore, this study serves as a proof-of-concept demonstration that rapid spray drying enables the concurrent achievement of high drug loading and physically stable CD-MOF structures, which highlights the potential of this approach. Both hydrophobic etodolac (ETD; Scheme 1B) and hydrophilic theophylline (THP; Scheme 1C) were selected as representative drugs, and their influence on the formation of CD-MOF particles was assessed. We aim (i) to quickly produce efficient drug-loading particles by spray drying, (ii) to evaluate the influence of drug loading on the stability of the CD-MOF structure, and (iii) to mechanistically understand the CD-MOF formation in presence of drugs using NMR and Raman spectroscopies.

Experimental

Materials

Crystalline etodolac (ETD; hydrophobic drug; log*P* 3.43) and anhydrous theophylline (THP; hydrophilic drug; log*P* −1.84) were purchased from Tokyo Chemical Industry (Tokyo, Japan). The log*P* values were calculated using ChemDraw v23.1 (PerkinElmer, MA). Powder X-ray diffraction patterns (XRD) of ETD and THP agreed with their respective calculated patterns from the CSD (refcode: JUKNAH and BAPLOT01). For CD-MOF preparation, γ-cyclodextrin (γ-CD) and potassium hydroxide (KOH) were purchased from Tokyo Chemical Industry and Fujifilm Wako Pure Chemical (Osaka, Japan), respectively. For comparison, amorphous ETD was prepared by melt-quenching. Crystalline ETD was heated to 156 °C, held for 1.5 min, quench-cooled with liquid nitrogen, and characterized for amorphous halo using XRD. Amorphous THP could not be obtained because of the high crystallization propensity. THP monohydrate was synthesized by slurry conversion for 2 weeks and the dried powder were characterized using XRD.

Spray drying

CD-MOF and CD inclusion systems were prepared by spray drying (B-290, Büchi, Flawil, Switzerland). Table S1 lists the precursor mixture compositions. Each of γ-CD and KOH was completely dissolved in 24 mL of water at a 1 : 8 molar ratio. Following the addition of 16 mL of ethanol (40% v/v) at 2 mL min^{-1}, a total of 40 mL of mixture was stirred and processed by spray drying at a feed rate of 5.5 mL min^{-1}. For the drug-containing particles, THP and ETD were added and dissolved in initial water and ethanol, respectively. The inlet temperature was maintained at 130 °C, which resulted in an outlet temperature of ~70 °C.

Anti-solvent crystallization

For comparison with spray-dried CD-MOFs, general anti-solvent crystallization of CD-MOFs was performed. Similarly processed precursor mixture (40 mL) was stirred at 900 rpm for 1 h and left at 50 °C for 1.3 h. The CD-MOF crystal was then precipitated at 0 °C for 22 h. The collected crystal was placed under vacuum at 20 °C for 22 h to remove the residual solvent.

Morphological analysis

Scanning electron microscopy (Miniscope TM3030, Hitachi, Tokyo, Japan) was used to study the particle morphology. The acceleration voltage and magnification were 15.0 kV and 5000×, respectively. The Brunauer–Emmett–Teller (BET) surface area was measured by nitrogen adsorption/separation isotherms of the powder samples at −196 °C (BELSORP MINI X, MicrotracBEL, Osaka, Japan). The samples were dried at 50 °C for 6 h.

Powder X-ray diffractometry

X-ray diffractometry patterns were collected at room temperature (SmartLab, Rigaku, Tokyo, Japan) using Cu Kα radiation (30 kV, 15 mA). The 2θ angular range was 3–33° with a step size of 4° min^{-1}.

High-performance liquid chromatography

High-performance liquid chromatography (HPLC) was used to analyse the drug concentration of samples after dilution with the mobile phase (Shimazu, Kyoto, Japan). The concentrations of ETD and THP were measured using a C18 column (4.6 μm × 150 mm, COSMOSIL 5C18-MS-II, Nacalai Tesque, Kyoto, Japan). The mobile phase of acetonitrile (0.1% trifluoroacetic acid with 60 : 40 and 15 : 85 volume ratio for ETD and THP, respectively) was flowed at 1.0 mL min^{-1} at 40 °C. The separated ETD and THP from 10 μL of injection were detected by UV absorbance at 272 nm.

Dissolution testing for 1 mg of the sample (drug equivalent) was performed in 10 mL water using a shaking bath (BW400, Yamato Scientific, Tokyo, Japan) at 100 shakes per min under non-sink conditions. Aliquots were removed at the desired timepoints, and the concentration of ETD and THP was measured by HPLC.

Nuclear magnetic resonance spectroscopy

Proton nuclear magnetic resonance (^{1}H NMR) spectroscopy was performed on a DD2 600 MHz spectrometer equipped with a variable-temperature controller (Agilent, CA). The chemical shifts were referenced to the methyl group of 3-(trimethylsilyl) propionic acid at 0 ppm and 25 °C. An accurately weighed amount of powder sample was dissolved in D_2O. NOESY spectra were recorded at a mixing time of 500 ms. The chemical shifts of ETD, THP, and γ-CD were predicted using ChemDraw v23.1 (PerkinElmer, MA) for the resonance assignments.

Raman spectroscopy

Raman spectroscopy imaging of spray-dried particles was obtained by a full achromatic micro confocal Raman spectrometer (LabRAM Odyssey, HORIBA, Kyoto, Japan) with an 800 mm focal length. The excitation laser wavelength and the output power were 633 nm and 15 mW, respectively. The spectral coverage was between 300 and 1800 cm^{-1}. Raman spectra were collected at a spatial resolution of 0.2 × 0.2 $μm^2$, with an exposure time of 10 s and 1 accumulation per point. The collected spectra were normalized using the peak intensity of γ-CD at 1120 cm^{-1}.

Results and discussion

The precursor mixture for spray drying consisted of ETD and THP, along with CD-MOF components [γ-CD and KOH (1 : 8 molar ratio)] in 40% ethanol (Table S1, SI). The ethanol concentration was optimized in a previous work.[19] Over 90% w/w drug-containing CD-MOF particles were produced in 30 min by spray drying. High drug-loading and drastic time reduction were simultaneously accomplished (Table 1).

Scanning electron microscopy showed that the CD-MOF particles prepared from spray drying and anti-solvent crystallization methods have spherical and block-like morphologies, respectively (Fig. 1 and S1–S3, SI). Moreover, the calculated Brunauer–Emmett–Teller (BET) surface area drastically increased in CD-MOF systems (Fig. S4, SI). The block shape was attributed to the highly crystalline CD-MOF formation with a larger specific surface area. Interestingly, ETD-containing spray-dried CD-MOF was characterized formation of cubic crystals on the surface due to the growth of CD-MOF crystals, in proportion with ETD concentration (Fig. 1). The ETD facilitated crystal growth of CD-MOF, generating a more porous surface morphology, which was reflected in the increased BET surface area.

Table 1 Concentration of (a) ETD and (b) THP in the prepared CD-MOFs (mean ± SD; n = 3). The weight ratio between the CD-MOF and drug is given in parenthesis

	ID (CD-MOF : ETD : THP)	Anti-solvent, % w/w	Spray drying, % w/w
(a) ETD	R1 (100 : 8 : 0)	23.1 ± 0.5	98.2 ± 0.7
	R2 (100 : 15 : 0)	19.3 ± 0.3	89.1 ± 4.8
	R3 (100 : 30 : 0)	18.6 ± 0.2	97.5 ± 2.7
	R7 (100 : 8 : 8)	NA	97.2 ± 1.0
	R8 (100 : 15 : 15)	NA	97.1 ± 0.2
	R9 (100 : 30 : 30)	NA	94.4 ± 1.8
(b) THP	R4 (100 : 0 : 8)	4.0 ± 0.1	91.4 ± 1.6
	R5 (100 : 0 : 15)	4.6 ± 0.2	95.4 ± 1.1
	R6 (100 : 0 : 30)	5.3 ± 0.1	96.7 ± 0.2
	R7 (100 : 8 : 8)	NA	97.8 ± 0.7
	R8 (100 : 15 : 15)	NA	98.4 ± 0.1
	R9 (100 : 30 : 30)	NA	96.2 ± 2.5

The crystal structure of CD-MOF was published in the Cambridge Structural Database (refcode: LAJLAL).[8,9] The experimental powder X-ray diffraction (XRD) pattern of the CD-MOFs exhibited characteristic peaks of calculated patterns at 2θ of 4°, 7°, and 13° (Fig. 2 and S5, SI). No peaks of ETD (at 9°, 19°, and 23°) and THP (at 12°, 26°, and 29°) were observed in the drug-containing systems, indicating the amorphous state of both drugs. Spray-dried particles showed

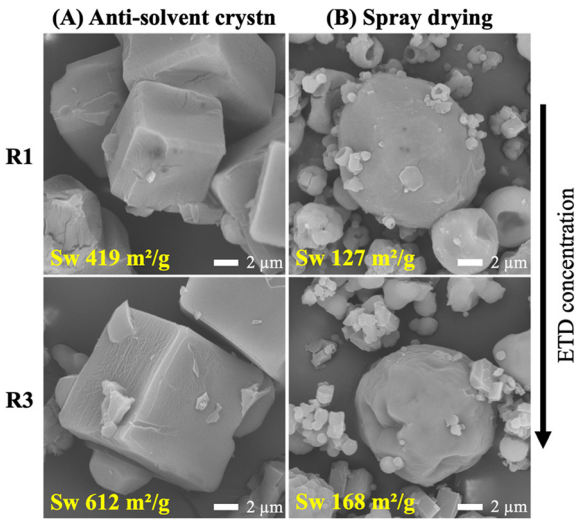

Fig. 1 SEM images and BET specific surface area of CD-MOFs containing ETD (R1, R3) prepared by (A) anti-solvent crystallization and (B) spray drying.

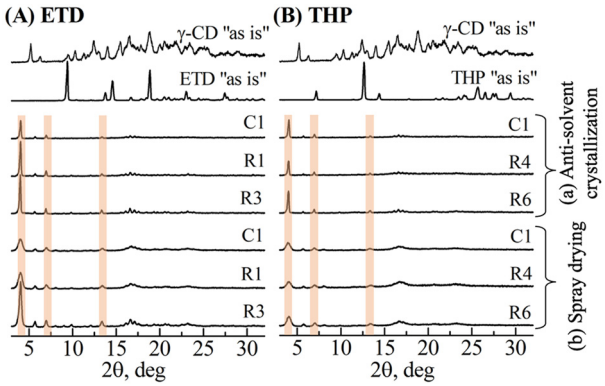

Fig. 2 Summarized XRD patterns of precursor materials and dried CD-MOFs with (A) ETD and (B) THP obtained by (a) anti-solvent crystallization and (b) spray drying. C1 refers to the drug-free samples. The ETD and THP concentrations are C1 < R1 < R3 and C1 < R4 < R6, respectively. The shaded areas show the peaks of the CD-MOF at 4°, 7°, and 13°.

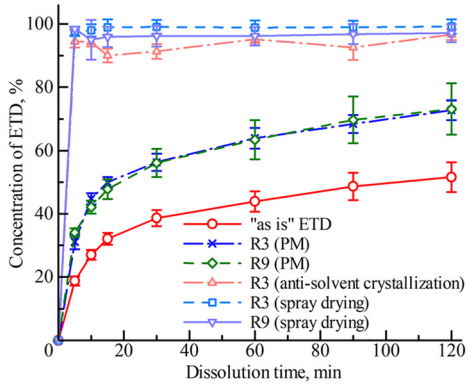

Fig. 3 ETD concentrations as a function of dissolution time in water following the dispersion of powder containing 1.0 mg of drug, physical mixture of γ-CD and drug (PM), and CD-MOF systems prepared by anti-solvent crystallization and spray drying (mean ± SD; n = 3).

low crystallinity and small crystallite sizes compared with the anti-solvent method.[27] As the ETD concentration increased, the intensity of the peaks attributed to the CD-MOF progressively increased. The crystal growth of CD-MOF agrees with the above morphological analysis. The ETD could be loaded at the hydrophobic space formed between two γ-CD molecules based on earlier simulation and experimental results.[28,29] ETD may have functioned as the linker and contributed to the crystal growth of CD-MOF.

The amount of loaded drugs in CD-MOFs prepared by spray drying and anti-solvent crystallization was significantly different (Table 1), with the spray drying method showing improved drug loading. The molecular size of ETD and THP was determined to be 0.96 × 0.92 nm^2 and 0.59 × 0.75 nm^2, respectively (Scheme 1B and C).[30,31] In the CD-MOF structure, γ-CD has a bucket-shaped hydrophobic cavity of 0.95 nm × 0.8 nm^2 (Scheme 1A).[9,11] The γ-CD units occupy the faces of a cube, and their primary faces point to the interior, forming a 1.70 nm produced by the anti-solvent crystallization method showed highly crystalline CD-MOFs with low drug loading (<20% w/w, Table 1). In a previous report, crystalline CD-MOF prepared by vapor diffusion contained approximately 20% w/w of 5-fluorouracil and ascorbic acid (model small-molecules) without pressure force.[15] The drug encapsulation capacity in rigid pores is limited because of the molecular size. Many drugs are organic compounds with a molecular weight over 100 g mol^{-1}. In contrast to anti-solvent crystallization method, we efficiently produced CD-MOFs contained a high loading of ETD and THP using spray drying (>90% w/w, Table 1). This could be explained by the slightly crystalline CD-MOF structure obtained *via* spray drying, wherein phase transition occurred from amorphous to thermodynamically stable crystal due to prompt solvent evaporation. During this process, ETD and THP were trapped in the center and linker section of the $(\gamma\text{-CD})_6$ cubic crystal which provide hydrophobic and hydrophilic cavities, respectively. The slightly crystalline structure is unique to spray-dried particles; thus, highly drug-loaded particles were obtained. Compared with conventional vapor diffusion and anti-solvent crystallization methods, which typically require long preparation times and yield limited drug loading, our spray-drying approach achieved rapid formation of CD-MOFs within 30 min while maintaining high drug loading (Table S2, SI).[15,18,32] These results indicate clear evidence of the advantage of spray drying as a scalable and efficient route for pharmaceutical applications. Additionally, the spray dried CD-MOFs showed excellent immediate drug release and reached complete dissolution within 5 min (Fig. 3 and S6, SI). The poor-water solubility of ETD was drastically improved by its inclusion in the CD-MOF carrier.

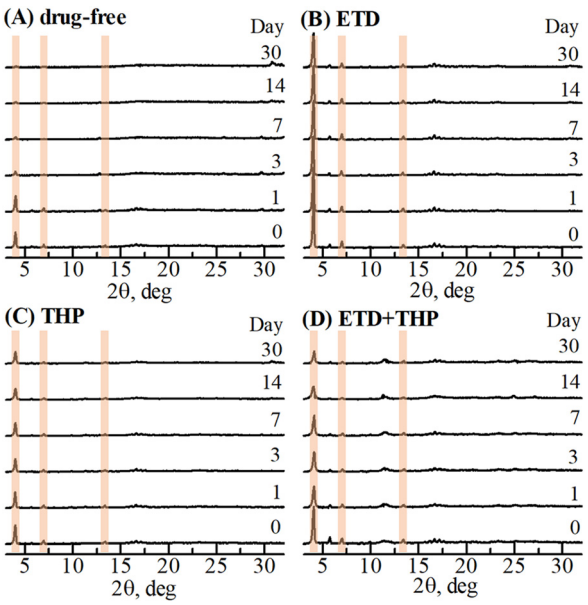

Fig. 4 Powder XRD patterns of spray-dried CD-MOFs stored at 40 °C and sealed condition. Spray drying was carried out with (A) drug-free (C1), (B) ETD (R3), (C) THP (R6), and (D) ETD and THP (R9). The shaded areas show the peaks of the CD-MOF at 2θ = 4°, 7°, and 13°.

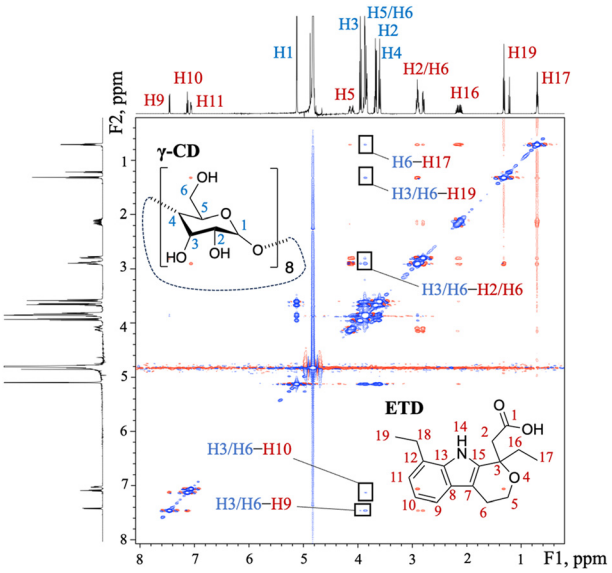

Fig. 5 Two-dimensional $^{1}H\{^{1}H\}$ NOESY plot of a CD-MOF containing γ-CD and ETD (R3) in D_2O. Cross peaks framed in black between the γ-CD and ETD peaks indicate intermolecular interactions.

Accelerated physical stability testing of the spray-dried particles was carried out at 40 °C/sealed and 40 °C/75% RH environments (Fig. S7 and S8, SI). At 40 °C/75% RH, spray-dried CD-MOF particles were easily deliquesced within 1 h due to their large surface area, while the ETD-containing systems retained the CD-MOF structure even in humid storage until 1 month. In case of the 40 °C/sealed environment, CD-MOFs without drugs were gradually disordered and characteristic peaks of CD-MOF almost disappeared after one month (Fig. 4A). The crystallinity of γ-CD-MOF crystals has been reported to be susceptible to temperature and humidity.[7] However, in our drug-containing CD-MOFs, especially with ETD, the peak intensity of CD-MOF at 2θ of 4°, 7°, and 13° were maintained until 1 month (Fig. 4 and S9, SI).

The molecular state of ETD and THP in the CD-MOF was investigated by ^{1}H NMR spectroscopy and Raman spectroscopic imaging. Two-dimensional (2D) $^{1}H\{^{1}H\}$ nuclear Overhauser effect spectroscopy (NOESY) was used to probe the molecular interactions in detail (Fig. 5). The ^{1}H NMR spectrum of ETD showed characteristic peaks attributed to H17, H19, H2/H6, H10, and H9 (Fig. 2). In NOESY analysis of CD-MOF with ETD, cross peaks (framed in black) between the proton peaks of ETD and those of γ-CD at H4, H2, H5/H6, H3, and H1 revealed the spatial proximity of the ETD and γ-CD molecules. These results suggest the existence of ETD–CD interaction and ETD was included in the hydrophobic inner space of γ-CD (Scheme 2). Therefore, the ETD in the CD-MOF cavities serve as the linker between γ-CDs to form the structure and improve the physical stability of the CD-MOF crystal (Fig. 4). Conversely, when the THP was formulated into CD-MOF, there were no cross peak assignment in the NOESY, indicating that hydrophilic THP was not housed in the hydrophobic interior of γ-CD (Fig. S10, SI).

Raman spectroscopy imaging was employed to identify the state of drugs in the spray-dried particle. Intense Raman peaks at 1680 cm^{-1} and 1580 cm^{-1} were attributed to carbonyl C=O stretching vibration of THP and aromatic ring C–C stretching vibration of ETD, respectively confirming drug loading (Fig. 6).[33,34] The spatial distribution of drugs in a spray-dried microsphere was then obtained using these Raman peaks (Fig. 6 and S11, SI). Both drugs were dispersed homogeneously in the particle. No such homogeneous dispersion was observed in the CD inclusion complexes. Furthermore, the ETD peak was broadened by amorphization, and the calculated peak width (full-width at half-maximum) was increased in ETD-containing. CD-MOF (Fig. 7). This peak broadening agrees with an earlier report, suggesting drug–CD interaction.[35] Fig. S12 (SI) shows the distribution of ETD in the particle using the peak width,

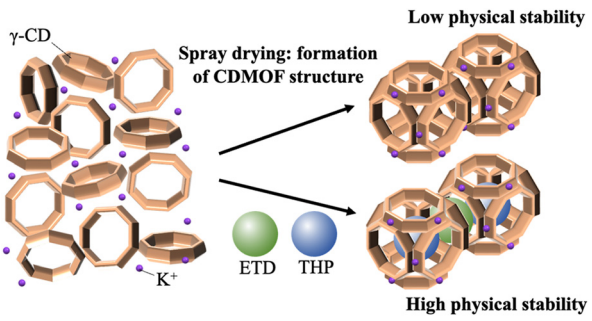

Scheme 2 Representation of CD-MOF formation in the absence (top right) and presence (bottom right) of drugs *via* spray drying.

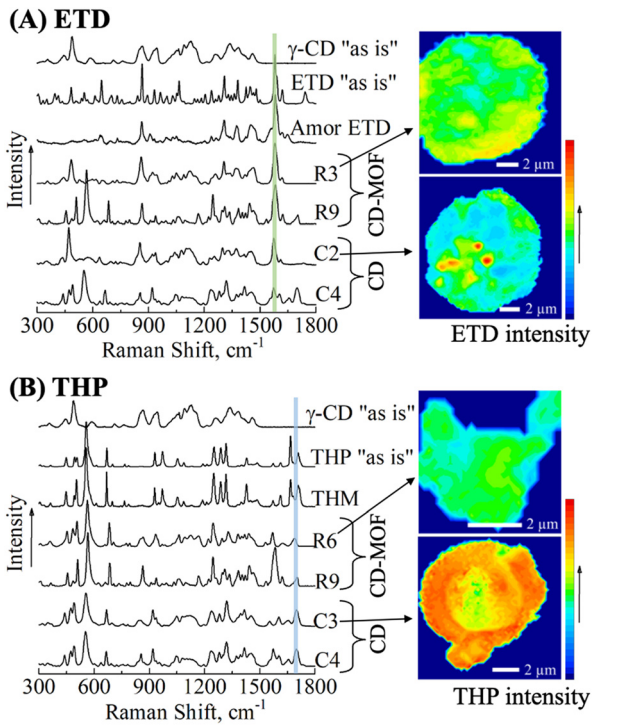

Fig. 6 Raman spectra of materials and prepared CD and CD-MOF systems containing (A) ETD or (B) THP. 2D Raman images of CD (C2, C3) and CD-MOF systems (R3, R6) were obtained using the highlighted ETD and THP peaks at 1580 cm^{-1} and 1680 cm^{-1}, respectively.

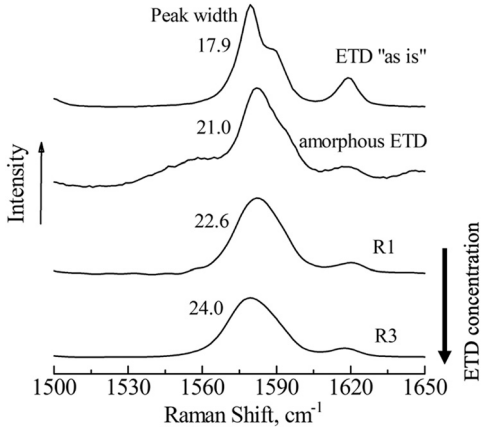

Fig. 7 Raman spectra of "as is" ETD, amorphous ETD, and CD-MOF (R1, R3). The calculated peak width (full-width at half-maximum) at 1580 cm^{-1} is shown in the graph.

confirming the homogeneous dispersion and interaction of ETD with γ-CD. This study serves as a foundational proof of concept and that the versatility of the approach with other guest molecules is a subject for future investigation.

Conclusions

In summary, stable cyclodextrin metal–organic frameworks (CD-MOFs) containing both hydrophobic etodolac (ETD) and hydrophilic theophylline (THP) were successfully prepared by spray drying within 30 min. This drug-assisted amorphous–crystal phase transition in CD-MOF significantly shortened synthesis time and enhanced drug loading compared with conventional anti-solvent crystallization. Importantly, ETD functioned as a molecular linker between γ-CD units, contributing to the structural stability of the CD-MOFs. Our findings provide proof-of-concept that spray drying with drug assistance enables the rapid and efficient preparation of stable CD-MOFs. This integrated approach, which combines spray drying, molecular-level insights obtained through NMR and Raman analysis, and the achievement of high drug loading with structural stability, underscores the potential of spray drying as a scalable technique for the pharmaceutical application of CD-MOFs.

Author contributions

R. Tanaka: conceptualization, methodology, investigation, data curation, formal analysis, writing-original draft, writing-editing & reviewing, and project administration, M. N.: investigation, data curation, and formal analysis, R. Togashi: investigation and data curation, K. M.: investigation, data curation, and formal analysis, H. U.: writing-editing & reviewing, S. T.: conceptualization, data curation and writing-editing & reviewing, Y. T.: conceptualization, writing-editing & reviewing, project administration, and supervision, K. K.: conceptualization, methodology, writing-editing & reviewing, project administration, and supervision.

Conflicts of interest

There are no conflicts to declare.

Data availability

The data supporting this article have been included as part of the supplementary information (SI).

Supplementary information: composition of samples, benchmarking, SEM images, BET analysis, XRD, dissolution profile, NMR, and Raman imaging. See DOI: **https://doi.org/10.1039/d5ce00755k**.

Acknowledgements

We express our appreciation to HORIBA for providing the LabRAM Odyssey. We also thank Mr. Yuta Ando and Ms. Peiwen Mo at Osaka Medical and Pharmaceutical University for their experimental help. This research was partially supported by the JSPS KAKENHI grant (23K06245 and 25K23784).

References

1 H.-L. Jiang and Q. Xu, *Chem. Commun.*, 2011, **47**, 3351–3370.
2 C. Jiang, X. Wang, Y. Ouyang, K. Lu, W. Jiang, H. Xu, X. Wei, Z. Wang, F. Dai and D. Sun, *Nanoscale Adv.*, 2022, **4**, 2077–2089.
3 S. Tanaka, K. Fujita, Y. Miyake, M. Miyamoto, Y. Hasegawa, T. Makino, S. Van der Perre, J. Cousin, S. Remi, T. Van Assche, G. V. Baron and J. F. M. Denayer, *J. Phys. Chem. C*, 2015, **119**, 28430–28439.
4 J. L. Obeso, J. G. Flores, C. V. Flores, M. T. Huxley, J. A. de los Reyes, R. A. Peralta, I. A. Ibarra and C. Leyva, *Chem. Commun.*, 2023, **59**, 10226–10242.
5 M. C. Scicluna and L. Vella-Zarb, *ACS Appl. Nano Mater.*, 2020, **3**, 3097–3115.
6 J. M. Holcroft, K. J. Hartlieb, P. Z. Moghadam, J. G. Bell, G. Barin, D. P. Ferris, E. D. Bloch, M. M. Algaradah, M. S. Nassar, Y. Y. Botros, K. M. Thomas, J. R. Long, R. Q. Snurr and J. F. Stoddart, *J. Am. Chem. Soc.*, 2015, **137**, 5706–5719.
7 B. Liu, H. Li, X. Xu, X. Li, N. Lv, V. Singh, J. F. Stoddart, P. York, X. Xu, R. Gref and J. Zhang, *Int. J. Pharm.*, 2016, **514**, 212–219.
8 R. A. Smaldone, R. S. Forgan, H. Furukawa, J. J. Gassensmith, A. M. Z. Slawin, O. M. Yaghi and J. F. Stoddart, *Angew. Chem., Int. Ed.*, 2010, **49**, 8630–8634.
9 R. S. Forgan, R. A. Smaldone, J. J. Gassensmith, H. Furukawa, D. B. Cordes, Q. Li, C. E. Wilmer, Y. Y. Botros, R. Q. Snurr, A. M. Z. Slawin and J. F. Stoddart, *J. Am. Chem. Soc.*, 2012, **134**, 406–417.
10 R. S. Forgan, R. A. Smaldone, J. J. Gassensmith, H. Furukawa, D. B. Cordes, Q. Li, C. E. Wilmer, Y. Y. Botros, R. Q. Snurr, A. M. Z. Slawin and J. F. Stoddart, *J. Am. Chem. Soc.*, 2012, **134**, 406–417.
11 I. Roy and J. F. Stoddart, *Acc. Chem. Res.*, 2021, **54**, 1440–1453.

12 K. Kadota, H. Uchiyama, T. Kämäräinen, S. Tanaka and Y. Tozuka, *Expert Opin. Drug Delivery*, 2024, **21**, 945–963.
13 X. Li, T. Guo, L. Lachmanski, F. Manoli, M. Menendez-Miranda, I. Manet, Z. Guo, L. Wu, J. Zhang and R. Gref, *Int. J. Pharm.*, 2017, **531**, 424–432.
14 K. J. Hartlieb, D. P. Ferris, J. M. Holcroft, I. Kandela, C. L. Stern, M. S. Nassar, Y. Y. Botros and J. F. Stoddart, *Mol. Pharmaceutics*, 2017, **14**, 1831–1839.
15 A. Ohashi, K. Ohshima, S. Ohsaki, H. Nakamura and S. Watano, *Int. J. Pharm.*, 2025, **670**, 125104.
16 A. Ziaee, A. B. Albadarin, L. Padrela, T. Femmer, E. O'Reilly and G. Walker, *Eur. J. Pharm. Sci.*, 2019, **127**, 300–318.
17 L. A. Miller, R. L. Carrier and I. Ahmed, *J. Pharm. Sci.*, 2007, **96**, 1691–1707.
18 J. Y. Tse, K. Kadota, T. Nakajima, H. Uchiyama, S. Tanaka and Y. Tozuka, *Cryst. Growth Des.*, 2022, **22**, 1143–1154.
19 K. Kadota, J. Y. Tse, S. Fujita, N. Suzuki, H. Uchiyama, Y. Tozuka and S. Tanaka, *ACS Appl. Bio Mater.*, 2023, **6**, 3451–3462.
20 A. Carné-Sánchez, I. Imaz, M. Cano-Sarabia and D. Maspoch, *Nat. Chem.*, 2013, **5**, 203–211.
21 S. Tanaka and R. Miyashita, *ACS Omega*, 2017, **2**, 6437–6445.
22 S. Elli, M. Caruso, A. Sacchetti and J. Martí-Rujas, *RSC Mechanochem.*, 2025, **2**, 188–192.
23 A. Ghazy, M. Safdar, M. Lastusaari and M. Karppinen, *Chem. Commun.*, 2020, **56**, 241–244.
24 M. F. Thorne, C. Castillo-Blas, L. N. McHugh, A. M. Bumstead, G. Robertson, A. F. Sapnik, C. S. Coates, F. N. Sayed, C. P. Grey, D. A. Keen, M. Etter, I. da Silva, K. Užarević and T. D. Bennett, *Chem. Commun.*, 2022, **58**, 11949–11952.
25 P. Su, H. Tang, M. Jia, Y. Lin and W. Li, *AIChE J.*, 2022, **68**, e17576.
26 S. A. Mohamed and J. Kim, *J. Phys. Chem. C*, 2021, **125**, 4509–4518.
27 P. Mo, Y. Hatanaka, S. Ohta, Y. Nakayama, Y. Mawatari, S. Yamanaka, K. Minoura, M. Doi, H. Uchiyama, K. Kadota and Y. Tozuka, *Cryst. Growth Des.*, 2025, **25**, 4283–4294.
28 W. Zhang, T. Guo, C. Wang, Y. He, X. Zhang, G. Li, Y. Chen, J. Li, Y. Lin, X. Xu, L. Wu, S. Zhang and J. Zhang, *Pharm. Res.*, 2019, **36**, 117.
29 Y. He, W. Zhang, T. Guo, G. Zhang, W. Qin, L. Zhang, C. Wang, W. Zhu, M. Yang, X. Hu, V. Singh, L. Wu, R. Gref and J. Zhang, *Acta Pharm. Sin. B*, 2019, **9**, 97–106.
30 S. K. Rai, S. Allu and A. K. Nangia, *Cryst. Growth Des.*, 2020, **20**, 4512–4522.
31 Y. Ebisuzaki, P. D. Boyle and J. A. Smith, *Acta Crystallogr., Sect. C: Cryst. Struct. Commun.*, 1997, **53**, 777–779.
32 H. Li, N. Lv, X. Li, B. Liu, J. Feng, X. Ren, T. Guo, D. Chen, J. F. Stoddart, R. Gref and J. Zhang, *Nanoscale*, 2017, **9**, 7454–7463.
33 B. Amul, S. Muthu, M. Raja and S. Sevvanthi, *J. Mol. Struct.*, 2019, **1195**, 747–761.
34 H. Wikström, P. J. Marsac and L. S. Taylor, *J. Pharm. Sci.*, 2005, **94**, 209–219.
35 G. P. Blanch, M. L. Ruiz del Castillo, M. del Mar Caja, M. Pérez-Méndez and S. Sánchez-Cortés, *Food Chem.*, 2007, **105**, 1335–1341.